ELSEVIER

Chemical Engineering Journal 125 (2006) 25–33

Chemical Engineering Journal

www.elsevier.com/locate/cej

Crystallization of microscopic Y_2O_3 powders by different techniques of fluidization at high temperature

S. Alavi [a], N. Joffin [b], M. Vérelst [b], B. Caussat [a,*]

[a] *Laboratoire de Génie Chimique, UMR CNRS 5503, ENSIACET/INPT, 5 rue Paulin Talabot, BP 1301, 31106 Toulouse Cedex 1, France*
[b] *CEMES-CNRS, 29 rue Jeanne Marvig, 31055 Toulouse Cedex 4, France*

Received 1 December 2005; received in revised form 20 June 2006; accepted 7 August 2006

Abstract

A high temperature fluidized bed reactor (HTFBR) working at 900 to 1200 °C has been developed to crystallize microscopic yttria (Y_2O_3) powders synthesized by spray pyrolysis. Such crystallization is classically performed in crucible or in moving belt furnaces. In order to demonstrate the advantages of the fluidized bed process over the conventional static mode treatments, a comparative study of the main characteristics of particles after heat treatment in a crucible and in the HTFBR has been performed. The high interparticle forces existing in such Geldart group C powders made it necessary to activate their fluidization. Following previous results, two activated fluidization processes were studied: addition of coarse powders to fine particles and vibrated fluidization. The hydrodynamic behavior of these fluidized beds was analyzed through pressure drop measurements. Convenient fluidization conditions were obtained for the two activated fluidization processes, leading to isothermal beds. The size distribution, the crystallinity and the outer morphology of particles before and after thermal treatments were analyzed and compared for the three processes tested. Some pre-sintering phenomena occurred at 1200 °C, which were clearly more intense in crucible than in activated fluidization. The crystallinity of the samples treated was equivalent for the three methods of thermal treatment. The interest of fluidization processes to post-treat microscopic particles is thus fully demonstrated.

Keywords: Fluidization; Crystallisation; Microscopic powders; Microstructure; Vibrated fluidization; High temperature fluidized bed

1. Introduction

Phosphor materials play a key role in manufacturing emissive displays, paint pigments and high quality fluorescent lamps. Spray pyrolysis (SP) is one of the most efficient processes for the large scale production of microscopic phosphor particles. It should be noted that high temperature thermal post-treatments are mandatory to exalt the final properties of phosphors prepared by this technique. Indeed, the increase of crystallite size of the host lattice regardless of the surface area is essential to enhance the luminescent intensity of SP phosphor particles [1]. The size of the crystallites depends on the synthesis process parameters, e.g. the concentration of the solution, the temperature gradient along the SP column, etc. and on the temperature and the duration of the post-heat treatment [2–4].

This post-heat treatment is classically carried out in a static mode, for either a few grams of particles in a crucible at the lab scale or in moving belt furnaces at the industrial scale. The crystallization of most phosphor particles requires very high temperatures, e.g. between 900 and 1200 °C. The extreme temperatures associated with a static mode treatment often lead to sintering of particles. Sintering is the bonding of adjacent surfaces of particles, by heating most often below the melting point of the main constituent. Atomic diffusion through the welded areas is responsible for this bonding [5]. Here, sintering must be avoided since the sintered particles can no longer be used for the planned applications. Moreover, on an industrial scale, thermal gradients can exist across the powder deposited on the moving belt, which leads to heterogeneously crystallized particles.

In this framework, gas–solid fluidization appears to be an interesting alternative solution, since this technology involves intense mixing of particles by the gas flow, which could limit sintering phenomena. It naturally leads to isothermal conditions, which could improve the homogeneity of the final phosphor products. Fluidization is easy to scale up and can reach

* Corresponding author.
E-mail addresses: verelst@cemes.fr (M. Vérelst), brigitte.caussat@ensiacet.fr (B. Caussat).

1385-8947/$ – see front matter © 2006 Elsevier B.V. All rights reserved.
doi:10.1016/j.cej.2006.08.017

Nomenclature

D_v50	Volume median diameter of particles (μm)
DP*	Normalized pressure drop, i.e. dimensionless ratio of the experimental to the theoretical (weight of particles per cross-sectional area) pressure drop
T	Bed temperature (°C)
U	Superficial velocity of gas ($m\,s^{-1}$)
U_{mf}	Minimum velocity of fluidization ($m\,s^{-1}$)

high productivities, especially if organized in a continuous mode [6].

However, the main problem is that fluidization of microscopic powders belonging to Geldart group C particles [7] usually leads to slugging and channelling phenomena. The interparticle forces, especially Van der Waals forces, are considerable and govern the behavior of fine powder layers, which prevents their fluidization [8]. In order to improve this situation, fluidization can be activated by various means, using mixtures of fine and coarse powders, by applying mechanical stirring, exposing the bed to vibrations, etc. . . . [6]. Powder which is too fine to be fluidized on its own can be fluidized admixed with a sufficient quantity of coarser powders that can be fluidized on their own [9]. Dutta and Dullea [10] mixed a small amount of highly dispersed fluidizing aids into Geldart group C powders and found a significant reduction in the cohesivity of the powders. They suggested that by the addition of coarse powders, interparticle forces or particle interactions could be reduced. Mori and Yamamoto [11] investigated vibro-fluidization of Geldart group C powders and also mixtures of alumina particles of various sizes, covering Geldart C to A groups, with Geldart group C powders, and measured entrainment rates of these mixtures. They found that the entrainment rate depended strongly on mixed ratios and that the vibration prevented the progress of agglomeration as vibration amplitude and frequency increased. In contrast to other methods, the advantage of adding coarse to fine powders is that it is unnecessary to use additional equipment or devices. Alavi and Caussat [12] have studied the fluidization behavior of dense Y_2O_3 microscopic powders at ambient temperature and pressure. Different fluidization technologies were tested, such as mechanical stirred fluidization, vibrated fluidization and addition of easy-to-fluidize large particles. Stirred fluidization was not satisfactory. An improvement of the bed hydrodynamics was obtained by horizontally vibrating the column, for the highest vibration ratio strengths tested, i.e. 8.8. The vibration strength ratio is defined as the ratio of the vibration acceleration to that of gravity. Convenient fluidization conditions were found by adding 30 wt.% of dense alumina of 270 μm in mean diameter to microscopic powders. These results then opened the possibility of thermally post-treating such microscopic powders in a fluidized bed (FB).

It is well known that the bed temperature greatly influences the viscosity and density of the gas, resulting in an increase in the superficial gas velocity in the bed [13]. So far, few experimental studies relating to the heat treatment of microscopic powders at temperatures higher than 900 °C have been reported. These studies mainly focus on discussing the effect of temperature on the transition regime from bubbling to turbulent fluidization [14–19]. They show that conventional understanding and assumptions developed under ambient conditions possibly no longer apply to high temperature FB. Particularly for a FB of fine particles, it was suggested that not only the gas but also the interparticle forces are considerably affected by the bed temperature. According to Rietema and Piepers [20], the major interparticle forces influencing the fluidization of Geldart group C powders are Van der Waals, capillary and electrostatic forces. Very often, the most intense forces are Van der Waals ones. By increasing the temperature of the FB, the electrostatic and the capillary forces disappear, but the Van der Waals forces remain.

Europium-doped yttria (Y_2O_3:Eu) discovered decades ago, is still considered to be one of the best inorganic red phosphors, due to the sharp emission ($\lambda = 611$ nm) of the europium ion activator (Eu^{3+}) in the host lattice (Y_2O_3) and its excellent luminescence efficiency and stability [21]. These remarkable properties only appear after crystallization of Y_2O_3:Eu formed by SP [22].

In the present work, a high temperature fluidized bed reactor (HTFBR) was used to crystallize Y_2O_3 microscopic powders synthesised by SP as reported elsewhere [22]. The very high cost of europium imposed the use of undoped Y_2O_3 powders for this experimental study, as large amounts of particles were needed. However, the thermo-chemical properties of europium-doped and -undoped Y_2O_3 are very similar. It is well known that the partial substitution of Y^{3+} by the dopant Eu^{3+} in cubic Y_2O_3 leads to very small modifications of the chemical and physical properties of the matrix, so pure Y_2O_3 is a very good model for the red phosphor [23].

In order to reveal any advantage of the FB process over the conventional static mode heat treatment, a comparative study of the main particle characteristics after heat treatment in a crucible and in the HTFBR was performed. Following previous results [24], two activated fluidization processes were studied: addition of coarse to fine powders and vibrated fluidization. The size distribution, the crystallinity and the outer morphology of the Y_2O_3 particles before and after thermal treatment were analyzed. Prior to these post-treatments, the fluidization behavior of these Geldart group C powders was studied between 900 and 1200 °C, in order to verify that the activated fluidization processes considered were able to fluidize microscopic powders and then to ensure isothermal treatment.

2. Experimental

2.1. High temperature fluidized bed reactor

Fig. 1 illustrates the experimental HTFBR used, consisting first of a cylindrical alumina column; its internal diameter and its height were 0.05 and 1.2 m, respectively. A porous alumina plate provided a homogeneous gas distribution. A long wide box underneath acted as a pre-heater for the fluidizing gas. Water cooled flanges located at the bottom and top parts of the column ensured the tightness of the reactive zone.

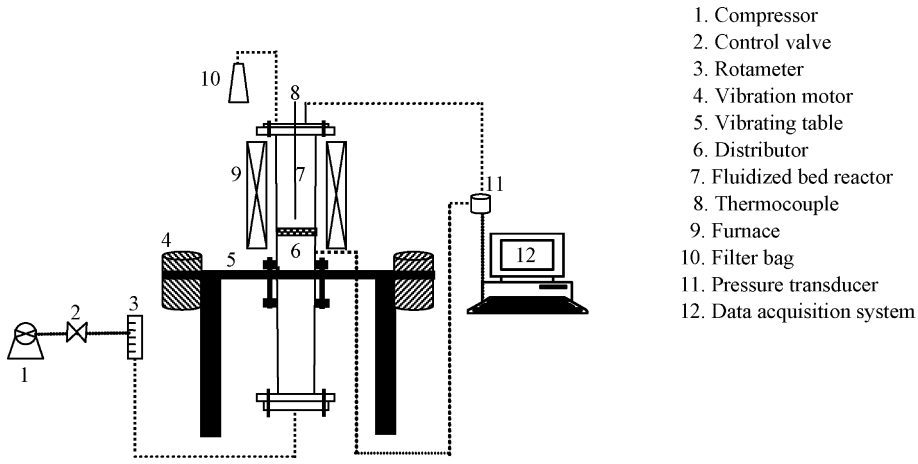

Fig. 1. Schematic representation of the high temperature fluidized bed reactor (HTFBR).

The reactor was externally heated by a three-zone electrical furnace able to operate at temperatures up to 1300 °C. Three regulating thermocouples were placed on the outer reactor wall. FB temperatures were monitored using a movable-central thermocouple which indicated the axial profile of temperature in the reactor. A fast response differential pressure gauge controlled the pressure drop existing between the bottom part of the reactor (under the distributor) and its top part. For security reasons, an absolute pressure gauge measured the total pressure under the distributor.

The experiments were performed at ambient pressure. The differential pressure drop and FB temperature were monitored continuously using a computerized data acquisition system. Dry air was used as the fluidizing gas. Its flow rate was controlled by a calibrated rotameter. A bag filter was located after the reactor exit to collect the elutriated particles.

Vibrated fluidization experiments were performed by fixing the FB column on a vibrating table as illustrated in Fig. 1. Two vibro-motors were cross-mounted on the opposite sides of the vibrating table. In order to obtain perfect horizontal vibrations, the centre of gravity of the column was adjusted to be level with the motors. The vibration amplitude was fixed by varying the eccentric weights on the vibro-motors and their frequency was controlled by an inverter. The vibration frequency could be varied from 19 to 25 Hz and the amplitude from 0.5 to 10 mm.

The experiments which involved adding large particles to fine powders were carried out in the HTFBR without exerting any external action.

A photograph of the experimental set up for the static mode treatment is presented in Fig. 2. A closed furnace of 40 cm × 40 cm × 40 cm was used, made up of four heating elements allowing a maximum temperature of 1500 °C to be reached. The sample was heated in a crucible of 6 cm in length, 2 cm in width and 1 cm in height, which was placed on the bottom of the furnace under confined air atmosphere.

2.2. Operating protocols and conditions

In all thermal treatments, the temperature was raised at a constant rate of 10 °C/min. When the thermal regime was reached, the crystallisation/densification process was maintained for

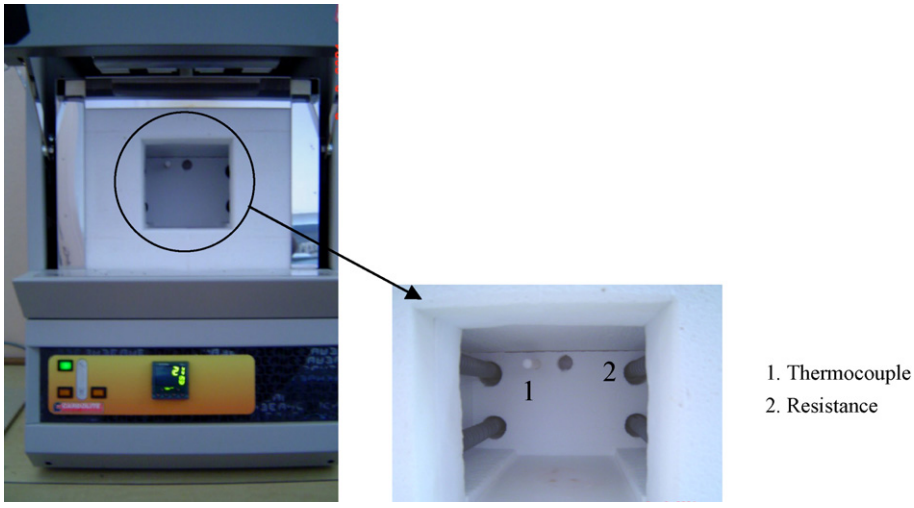

Fig. 2. Photograph of the set up for the static mode treatment (side view).

30 min as determined from previous results [22]. The operating temperatures were fixed at 900, 1000, 1100 and 1200 °C.

For the two activated fluidization techniques, the optimal fluidization conditions obtained at ambient temperature [12], were applied in this study at high temperature.

Concerning the operating procedure, for vibrated FB experiments, a mass of 300 g of Y_2O_3 was introduced into the HTFBR, corresponding to an initial fixed bed height of 20 cm. When coarse powders were used as fluidization promoters, pre-mixed weights of 140 g of Y_2O_3 and 140 g of group B porous alumina were introduced into the reactor. A constant flow rate of air fluidized the bed during its heating. When vibrated fluidization experiments were performed, vibrations were started at the same time as the heating. In all cases, the fluidization ratio U/U_{mf} was fixed to 1.1, so as to limit elutriation.

Minimum fluidization velocities of all the powders were determined classically by pressure drop measurements at decreasing gas velocities. They correspond to the intersection of the fixed bed zone with the fluidization plateau.

The frequency of pressure drop acquisition was 1 Hz. Each measured pressure drop in this study corresponds to an average value calculated over a period of 15 s before changing the operating conditions. The results are presented below in terms of normalized pressure drop (DP^*) corresponding to the experimental value divided by the theoretical one (i.e. weight of particles per surface area).

In activated fluidization processes, the weight of elutriated particles was systematically measured for each series of experiments from the difference between the initial and the final mass of particles in the reactor.

In all static crystallization runs, the crucible was filled with 5 g of Y_2O_3.

2.3. Characterization methods

Before and after each thermal treatment, the particles in the crucible and in the fluidized bed were characterized by the following techniques:

- Laser scattering size analyzes of particles put in ultrasonicated water dispersions were performed with a MasterSizer Malvern S set up. More precisely, the system uses water into which the powder is dispersed by mechanical stirring. Ultrasonic action is available to disperse cohesive materials. Both stirring and ultrasonication speeds are controllable to allow optimum transport and de-aggregation. For Y_2O_3, the stirring velocity was 1400 rpm and the ultrasonication was applied at a frequency of 20 kHz and amplitude of 20 μm. Each measurement corresponds to an average value calculated over three runs.
- The powder morphology was observed by field emission gun scanning electron microscopy (FEG SEM) on a JEOL 6700F.
- The powder X-ray diffraction (XRD) patterns were analyzed by a Seifert XRD3000 diffractometer using Cu Kα radiation in conventional operating conditions and $\theta = 2\theta$ configuration to analyze the crystalline phase. The JCPDS database and PowderCell diffraction pattern simulation software were used classically for identifying the phase diffraction peaks. The Scherrer crystallite size was estimated by the Halder, Schoenig and Wanger method [25].
- The particle apparent density was measured by water pycnometry and the Hausner ratio was determined in a Hosokawa powder tester.

2.4. Characteristics of initial powders

The cohesive powder studied was porous yttrium oxide or yttria (Y_2O_3) synthesized by SP in the Material and Elaboration Center (CEMES) in Toulouse, France, as reported elsewhere [4,22]. It has a volume median diameter of 1.8 μm. The particle apparent density was measured at 3.7 g cm^{-3}. This powder is hydrophilic. In addition, the Hausner ratio was 1.6, indicating that this powder is highly cohesive [26]. These parameters position the powder among Geldart group C particles, which cannot be fluidized by a classical fluidization method. We have verified that interparticle forces were so high that conventional fluidization was not possible: the bed of Y_2O_3 particles forms cracks and channels and the pressure drop variation versus gas velocity was quasi-linear.

Fig. 3 presents FEG SEM micrographs of the powder. These figures reveal a spherical morphology and a powder mainly formed of hollow particles. The figure reveals a shell thickness between 300 and 400 nm.

The coarse powder added to the fine Y_2O_3 powder used as fluidization promoter was Geldart group B porous alumina pur-

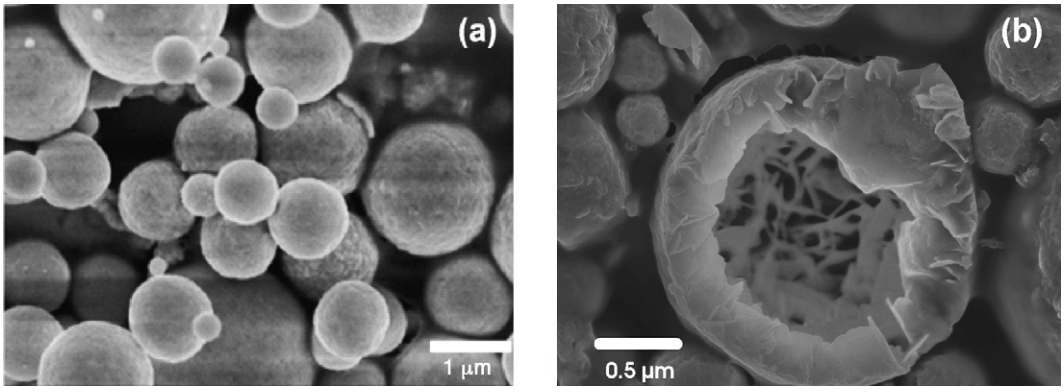

Fig. 3. (a and b) FEG SEM micrographs of the Y_2O_3 powder as produced by SP.

chased from Sasol. The volume median diameter of this coarse powder was 245 μm. Its apparent density was 2.5 g cm^{-3}. The Hausner ratio was 1.1, which confirmed the non-cohesivity of this group B powder. Its minimum fluidization velocity was 3.6 cm s^{-1} at ambient conditions.

3. Results and discussion

3.1. FB hydrodynamics at high temperature

The preliminary step before post-treating the Y_2O_3 particles was to analyze the hydrodynamic behavior of the FB between 900 and 1200 °C, then to measure the resulting axial profile of temperatures inside the FB, for the two processes of activated fluidization tested.

The variations of the normalized pressure drop with gas velocity for fixed temperatures of 900 and 1200 °C are given in Fig. 4.

It is clear that full fluidization conditions were reached for the two fluidization processes studied. The minimum fluidization velocity decreased as temperature increased. It varied between 0.7 and 0.9 cm/s STP (standard temperature and pressure) for the vibrated FB and from 0.7 to 2 cm/s STP when group B particles were added. From these criteria, the vibrated fluidization process is therefore more suitable for post-treating the Y_2O_3 particles, since it most often leads to lower gas consumption and a priori to lower particle elutriation. Indeed, during these hydrodynamic experiments, elutriation was about 6% of the initial bed weight when coarse powders were added and 4% in vibrated conditions. Particle elutriation was identical at the different temperatures. Moreover, as we will see in Section 3.2, another disadvantage is that the FB process activated by adding coarse powders necessitates an additional step after treatment, to separate the coarse powders from the microscopic ones.

The resulting axial temperature profiles in the FB for nominal temperatures fixed at 900 and 1200 °C are presented in Fig. 5 for the two activated fluidization processes. The data points presented in Fig. 5 are the averages of three runs. The results were identical for both activated processes.

These curves show that a uniform temperature was obtained in the FB from the distributor to the transport disengaging height,

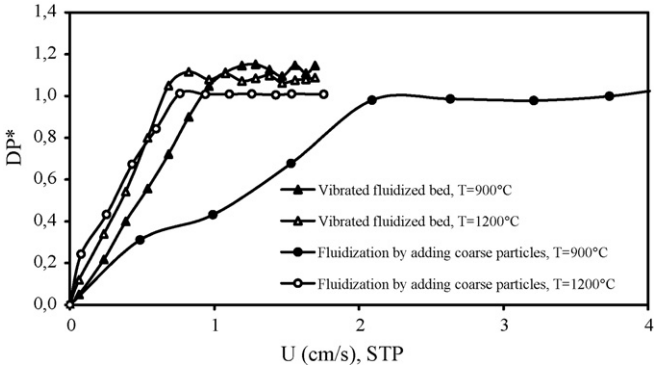

Fig. 4. Variations of the normalized pressure drop at decreasing gas velocities at fixed temperatures of 900 and 1200 °C for the two techniques of activated fluidization.

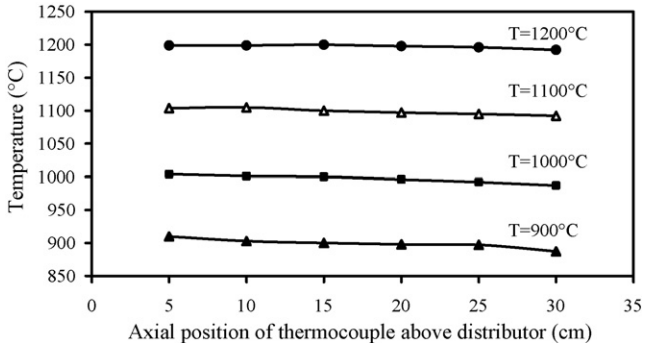

Fig. 5. Axial temperature profile along the reactor for different operating temperatures.

as a consequence of the satisfactory hydrodynamics of the FB previously mentioned.

The FB hydrodynamic and thermal characteristics involved in the two activated processes tested therefore appear as suitable for the crystallization of microscopic Y_2O_3 powders.

3.2. Separation of fluidizable powders from microscopic particles

One drawback of the FB process activated by adding coarse powders is that it is necessary to separate the group B particles from the microscopic ones after treatment. To ensure the industrial viability of this FB process, the efficiency of the separation must be 100%, given the high cost of microscopic phosphor particles. This objective is not easy to reach, due to the high cohesivity of such microscopic powders.

In this framework, different separation methods were studied on the basis of classical sieving. Classical lab-scale sieving equipment was used with only one sieve of 80 μm mesh, since the porous alumina particles had a size distribution between 90 and 310 μm. Twenty grams of mixture were treated per separation run with a vibrating frequency of 20 Hz for 10 min.

Sieving without adding any third body was tested first. Unfortunately, as reported in Table 1, the results were not satisfactory at all: a massive plugging of the sieve by the cohesive microscopic particles occurred. Various third bodies in the form of dense balls were then added to the mixtures of fine and coarse powders. Glass, alumina and stainless steel balls, 2 and 5 mm

Table 1
Separation of microscopic Y_2O_3 powders from group B alumina particles by sieving with and without a third body

Type of balls			Collected Y_2O_3 (wt.%)
Material	Diameter (mm)	Density (g/cm^3)	
Without third body	–	–	24
Stainless steel	2	7.9	100
Stainless steel	5	7.9	97
Alumina	2	3.9	78
Alumina	5	3.9	64
Glass	2	2.8	63
Glass	5	2.8	58

in diameter, were tested. The effects of density and diameter of these balls on the efficiency of sieving were studied.

The results prove the efficiency of adding a third body to prevent plugging of the sieve by the Y_2O_3 powders. The denser and smaller the balls, the higher the percentage of fine powders separated. The stainless steel balls of 2 mm in diameter were the most efficient for the mixtures tested since 100% of the Y_2O_3 present in the mixture was collected. The separation mechanisms probably involve mechanical effects: the balls may facilitate the crossing of the microscopic particles through the sieve by inertial effects. Larger ball sizes were less efficient in helping the powder cross the sieve.

These results are important since they stress the viability of the FB process activated by adding coarse powders.

3.3. Comparison of the various processes of thermal treatment

3.3.1. Crystallinity

Two crystalline phases exist for Y_2O_3, a cubic one and a monoclinic one. The cubic phase is stable over a large range of temperatures and pressures. This phase is the most sought after since it leads to the red phosphor material [4].

Fig. 6 shows the XRD patterns of Y_2O_3 particles as prepared by SP and after post-heat treatment at 1200 °C in a crucible and in the two FB processes. We observed that the XRD peaks sharpened with increasing temperature, indicating more intense crystallite growth. For all post-treated samples, the X-ray patterns correspond to the pure cubic Y_2O_3 phase according to the JCPDS database. There is no difference in product composition between the particles treated by the different techniques since the XRD peaks are the same.

For each spectrum, the six most intense diffraction peaks were analyzed to estimate the Scherrer crystallite size. They correspond to diffraction angles between 15° and 60°. As indicated in Fig. 7, in all cases, the Scherrer crystallite average size increased with temperature.

In the crucible as in the vibrated FB, the Scherrer size varied from 26 to 62 nm between 900 and 1200 °C. In all cases, the crystal size is the highest at 1200 °C. Joffin [4] has shown that the luminescence properties of Y_2O_3:Eu particles under plasma excitation are proportional to their final crystallite size. The temperature 1200 °C is then of interest to post-treat these particles.

In the FB activated with coarse powders, crystallization seemed to be slightly less efficient, since the Scherrer size varied between 24 and 55 nm for the same range of temperature. However, it is worth noting that this difference is within the error range of the characterization method. Under our tested conditions, the vibrated FB then appears to be as efficient in crystallizing these particles as the FB activated with group B particles.

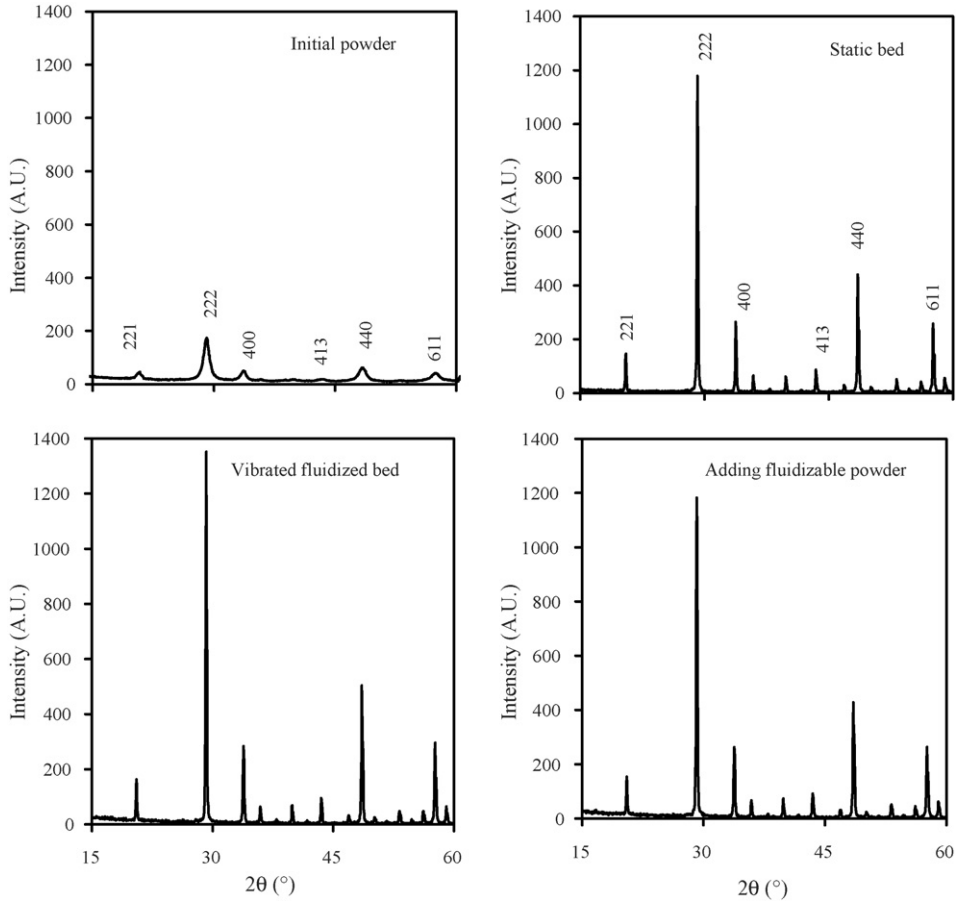

Fig. 6. XRD patterns of Y_2O_3 powder treated at 1200 °C by the various techniques.

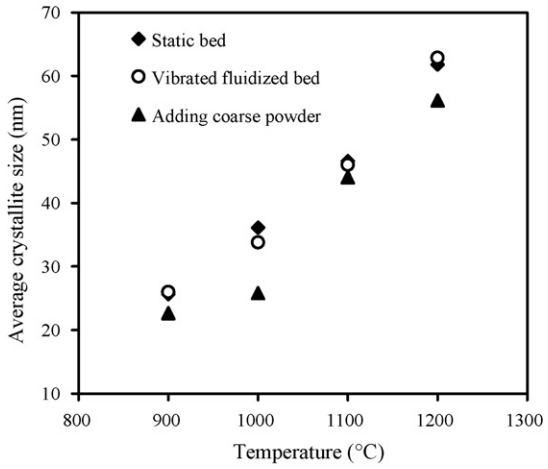

Fig. 7. Variation of the Scherrer crystallite size with operating temperature for the different post-treatment techniques.

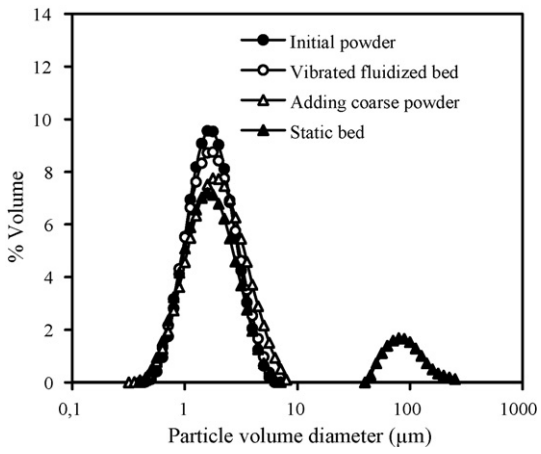

Fig. 8. Particle size distribution by laser scattering before and after thermal treatment at 1200 °C.

3.3.2. Particle size distribution

Table 2 gives the volume median diameter of the particles obtained by laser particle size measurements before and after post-treatment with the various processes.

It appears that the mean particle diameter remains constant at around 1.8 μm after all thermal treatments up to 1100 °C. At 1200 °C, a beginning of sintering (or pre-sintering) occurred for all processes and especially in crucible for which the mean particle diameter reaches 11 μm.

To clarify what occurred at 1200 °C, Fig. 8 gives the complete particle size distribution before and after heat treatment for the various processes.

It can be observed that, for the powders treated in FB, one population of particles exists, centred on a few micrometers. For the crucible treatment, an additional population of particles appears centred at 80 μm. This population probably corresponds to pre-sintered particles.

From the results as a whole, it can be concluded that the FB processes appear more efficient in limiting sintering than the conventional crucible treatment. The vibrated FB process seems to be slightly more efficient than the FB activated by coarse powders.

It should be recalled that all samples post-treated by FB activated with coarse powders, were sieved prior to analysis in order to remove the group B particles. A sieve of 80 μm mesh was used to separate the mixtures. In order to ascertain that this sieving did not mask possible sintering of Y_2O_3 particles, an additional particle size analysis was performed before sieving for the sample post-treated at 1200 °C. The particle size distributions obtained before and after sieving are given in Fig. 9.

Table 2
Volume median diameter of the particles treated by the various techniques vs. temperature

Temperature (°C)	Static bed	Vibrated fluidized bed	Fluidization by adding coarse powders
	D_v50 (μm)	D_v50 (μm)	D_v50 (μm)
25 (Initial powder)	2.0	2.0	2.0
900	2.2	1.8	1.8
1000	1.8	1.8	2.1
1100	1.9	1.8	1.8
1200	11.1	2.4	4.1

The results before sieving show a completely separated size distribution of Y_2O_3 and Al_2O_3 powders. The graphs prove that the size distribution of fine and coarse powders was not changed after post-heat treatment. No massive sintering occurred at 1200 °C with this technique. Therefore, no massive agglomeration occurred at lower operating temperatures (e.g. 900, 1000 and 1100 °C) in this process.

3.3.3. Surface morphology

The FEG SEM morphology of particles after post-heat treatment at 1200 °C by the three techniques studied is presented in Fig. 10.

Whatever the process used, the spherical morphology of the particles seems to be kept. No sintering of particles was observed. However, a few interparticle bridges were detected at 1200 °C whatever the process used. This confirms the phenomenon of pre-sintering previously mentioned.

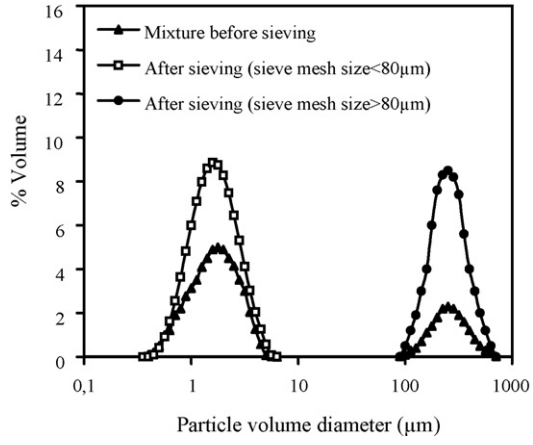

Fig. 9. Particle size distributions before and after sieving samples post-treated at 1200 °C in FB activated with coarse powders.

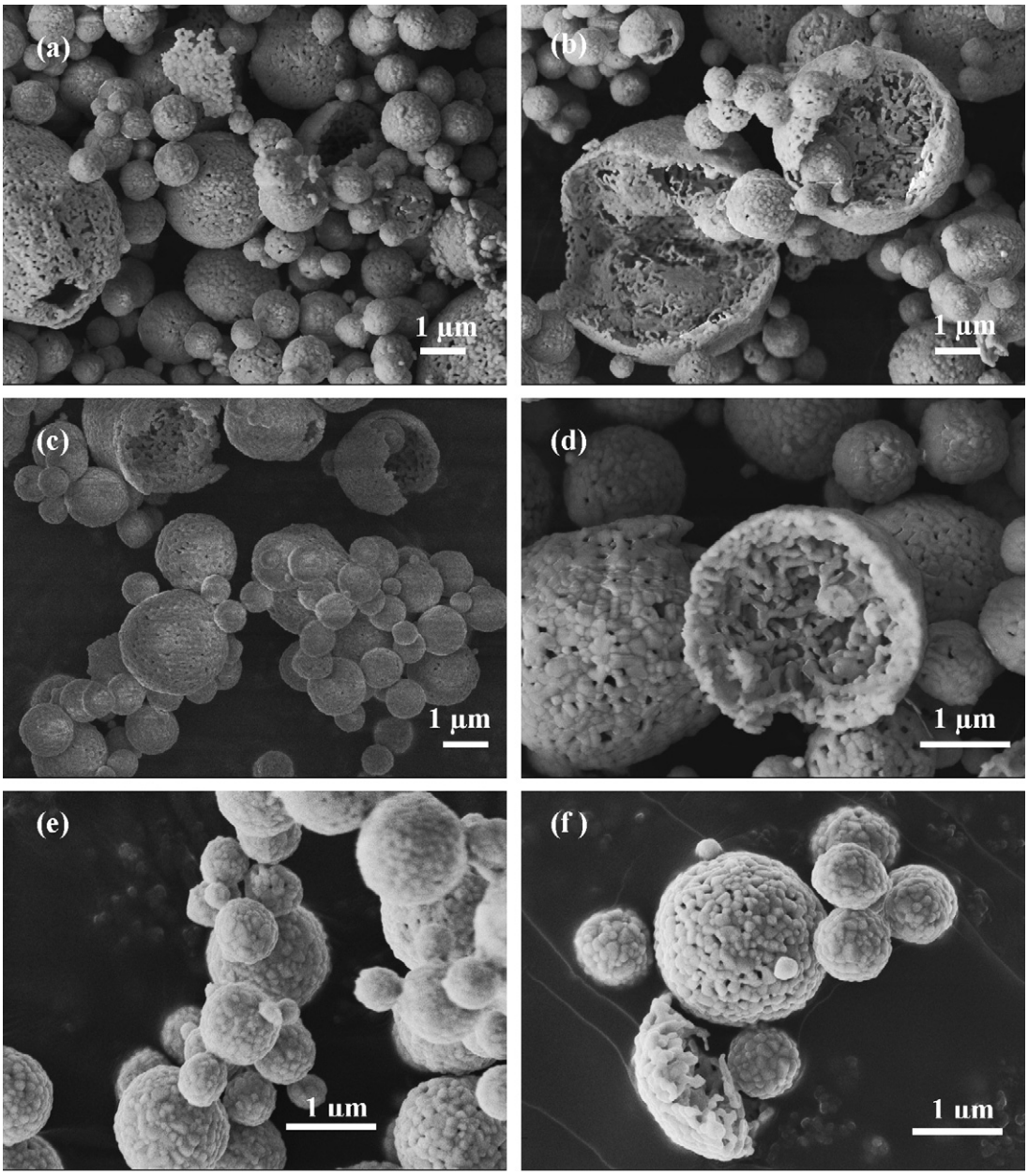

Fig. 10. FEG SEM views of the Y_2O_3 powders treated at 1200 °C: (a and b) thermal treatment in crucible; (c and d) thermal treatment in fluidized bed by adding fluidizable powders; (e and f) thermal treatment in vibrated fluidized bed.

The crystallization of the particle crust led to the formation of crystallized nodules instead of lamellae. Let us recall that the wall thickness was measured on the SEM micrographs as 300–400 nm for the particles at the exit of SP (Fig. 3). This thickness decreased to around 40–70 nm for the particles observed in Fig. 10. The wall thickness is a decisive parameter for luminescent properties of doped Y_2O_3 particles. On the one hand, 40–70 nm thickness is sufficient to ensure luminescence under visible ultra-violet (VUV) plasma excitation for flat plasma displays [22], and on the other hand, the hollowness of particles saves large amounts of expensive Y_2O_3 for a given specific surface area. The particles post-treated at 1200 °C are then particularly suitable for applications in flat emissive displays.

4. Conclusions

Microscopic porous Y_2O_3 powders have been treated at ambient air pressure between 900 and 1200 °C in order to crystallize and densify them to exalt their properties. Three heat treatment processes have been studied: (i) a conventional static bed process in a crucible, (ii) a fluidization process activated by adding coarse powders and (iii) another fluidization process activated by column vibrations.

This activation of the fluidization was necessary because of the high interparticle forces existing in such Geldart group C powders. The choice of these methods of activation proceeds from previous results obtained at ambient temperature.

First, the hydrodynamic behavior of these microscopic porous Y_2O_3 fluidized beds was surveyed through pressure drop measurements at decreasing gas velocities for the four temperatures of interest, 900, 1000, 1100 and 1200 °C. Convenient fluidization conditions were obtained for the two processes of activated fluidization, leading to isothermal beds.

The size distribution by laser scattering in water suspension with ultrasonication, the crystallinity by X-ray diffraction and the outer morphology by scanning electron microscopy of particles, before and after thermal treatments, have been analyzed and compared for the three processes tested.

The crystallinity of the samples treated was equivalent for the three methods of thermal treatment. The crystallite size increased with temperature for the conditions tested and was maximum at 1200 °C. The luminescence properties of Y_2O_3:Eu being proportional to the crystallite size under plasma excitation, 1200 °C is then the temperature of interest to post-treat this material.

Sintering started to occur at 1200 °C, clearly more intense in crucible than in the fluidization processes. Vibrated fluidization appeared to be slightly more efficient in limiting pre-sintering phenomena than fluidization activated by group B particles. Moreover, it most often led to lower gas consumption and lower elutriation than fluidization activated by adding coarse powders. Another drawback for the latter process is that it needs an additional separation step after treatment. An efficient sieving procedure has been proposed to recover 100% of the microscopic particles, consisting of adding an appropriate third body in the sieve.

These results open up promising perspectives for the post-treatment of microscopic powders in reproducible and uniform conditions in an easy-to-scale-up technology, i.e. the fluidization process, for crystallisation purposes, but also for their reduction, carbidization, grafting or even coating by chemical vapor deposition. Such fluidization processes could then be a very efficient means to improve the surface properties of microscopic particles of interest in wide fields of application.

Acknowledgements

The authors wish to thank Prof. J.P. Couderc and Dr. J. Dexpert-Ghys for their valuable contribution. This work was supported by the French Ministry of Research (RNMP/POSUMIC).

References

[1] K.Y. Jung, C.H. Lee, Y.C. Kang, Effect of surface area and crystallite size on luminescent intensity of Y_2O_3:Eu phosphor prepared by spray pyrolysis, Mater. Lett. 59 (19–20) (2005) 2451–2456.
[2] Y. Kang, S. Park, I. Lenggoro, K. Okuyama, Preparation of nonaggregated Y_2O_3:Eu phosphor particles by spray-pyrolysis method, J. Mater. Res. 14 (6) (1999) 2611–2615.
[3] H.G. Young, J.B. Soo, Y.Y. Kil, Y.J. Soo, Photoluminescence characteristics of spherical Y_2O_3:Eu phosphors by aerosol pyrolysis, J. Electrochem. Soc. 148 (11) (2001) H161–H166.
[4] N. Joffin, Ph.D. Thesis, Institut National Polytechnique de Toulouse, France, 2004.
[5] K. Linoya, K. Gotoh, K. Higashitani, Powder Technology Handbook, Second ed., Marcel Dekker Inc., New York, Basel, Hong Kong, 1991, pp. 379–383.
[6] D. Kuni, O. Levenspiel, Fluidization Engineering, Second ed., John Wiley & Sons Inc., New York, 1991, pp. 77–83.
[7] D. Geldart, Types of gas fluidization, Powder Technol. 7 (1973) 285–292.
[8] J. Visser, Van der Waals and the other cohesive forces affecting powder fluidization, Powder Technol. 58 (1989) 1–10.
[9] L. Eric, J. Ernest, Fluidizing fine powder, US patent, 4,379,186, 1983.
[10] A. Dutta, L.V. Dullea, Effect of external vibration and addition of the fibres on the fluidization of a fine powder, AIChE Symp. Ser. 93 (1994) 38–47.
[11] S. Mori, A. Yamamoto, Vibro fluidization of group-C particles and its industrial applications, AIChE Symp. Ser. 2 (1990) 88–94.
[12] S. Alavi, B. Caussat, Experimental study of fluidization of microscopic powders, Powder Technol. 157 (1–3) (2005) 114–120.
[13] H. Cui, P. Sauriol, J. Chaouki, High temperature fluidized bed reactor: measurements, hydrodynamics and simulation, Chem. Eng. Sci. 58 (2003) 1071–1077.
[14] J.E. Atwater, J.R. Akse, T.C. Wang, S. Kimura, D.C. Johnson, Preparation of silicon-carbide-coated activated carbon using a high temperature fluidized bed, Chem. Eng. Sci. 56 (8) (2001) 2685–2693.
[15] P. Cai, S.P. Chen, Y. Jin, Z.Q. Yu, Z.W. Wang, Effect of operating temperature and presssure on the transition from bubbling to turbulent fluidization, AIChE Symp. Ser. 85 (270) (1989) 37–43.
[16] A. Chehbouni, J. Chaouki, C. Guy, D. Klvana, Effect of temperature on the onset of turbulent fluidization, in: C. Laguerie, J.F. Large (Eds.), Fluidization VIII, Engineering Foundation, New York, 1995, pp. 149–156.
[17] H.T. Bi, J.R. Grace, Effects of pressure and temperature on the flow regimes in gas-solid fluidization system, Can. J. Chem. Eng. 74 (1996) 1025–1027.
[18] P.K. Peeler, K.S. Lim, R.C. Close, Effect of temperature on the turbulent fluidization regime transition, in: J. Werther (Ed.), Circulating Fluidized Bed Technology VI, Dechema, Frankfurt, 1999, pp. 125–130.
[19] P. Lettieri, D. Newton, J.G. Yates, The influence of interparticle forces on the fluidization behaviour of some industrial materials at high temperature, Powder Technol. 110 (2000) 117–127.
[20] K. Rietema, H.W. Piepers, The effect of interparticle forces on the stability of gas fluidized bed. I. Experimental evidence, Chem. Eng. Sci. 45 (1990) 1627–1639.
[21] C. Ronda, Recent achievements in research on phosphors for lamps and displays, J. Lumin. 72–74 (1997) 49–54.
[22] N. Joffin, J. Dexpert-Ghys, A. Garcia, M. Verelst, G. Baret, A. Garcia, The influence of microstructure on luminescent properties of Y_2O_3:Eu prepared by spray pyrolysis, J. Lumin. 113 (2005) 249–257.
[23] J. Dexpert, Ph.D. Thesis, Paris-Sud (Orsay) University, France, 1979.
[24] S. Alavi, Ph.D. Thesis, Institut National Polytechnique de Toulouse, France, 2004.
[25] B.E. Warren, X-ray Diffraction, Dover Publication Inc., New York, 1990, pp. 20–35.
[26] M.E. Fayed, L. Otten, Handbook of Powder Science and Technology, Van Nostrand Reinhold Company, 1984, pp. 394–398.